Automatika

Journal for Control, Measurement, Electronics, Computing and Communications

ISSN: (Print) (Online) Journal homepage: www.tandfonline.com/journals/taut20

Simplest and robust speed control for PMSMs with unknown mechanical characteristics

Abdelhak Djoudi, Seddik Bacha, Szymon Racewicz & Djamila Rekioua

To cite this article: Abdelhak Djoudi, Seddik Bacha, Szymon Racewicz & Djamila Rekioua (2024) Simplest and robust speed control for PMSMs with unknown mechanical characteristics, Automatika, 65:4, 1666-1676, DOI: 10.1080/00051144.2024.2429189

To link to this article: https://doi.org/10.1080/00051144.2024.2429189

Published online: 21 Nov 2024.

AUTOMATIKA
2024, VOL. 65, NO. 4, 1666–1676
https://doi.org/10.1080/00051144.2024.2429189

Simplest and robust speed control for PMSMs with unknown mechanical characteristics

Abdelhak Djoudi[a], Seddik Bacha[b], Szymon Racewicz[c] and Djamila Rekioua[d]

[a]CDER, Centre de Développement des Energies Renouvelables, Route de l'Observatoire Bouzeréah, Algiers, Algeria; [b]Grenoble INP, G2Elab, Univ. Grenoble Alpes, CNRS, Grenoble, France; [c]Faculty of Technical Sciences, University of Warmia and Masary in Olsztyn, Olsztyn, Poland; [d]Laboratoire de Technologie Industrielle et de l'Information, Université de Béjaia, ie, Faculté de Technologie, Bejaia, Algerie

ABSTRACT

This paper addresses speed control for permanent magnet synchronous machines (PMSMs), specifically focusing on the outer control loop within a cascaded control structure. The proposed approach aims to address the weaknesses of existing methods. One of its key advantages is that it does not require knowledge or estimation of mechanical torque, magnetic flux or inertia. Instead, it relies on a straightforward formula, avoiding the complex algorithms typically used to estimate mechanical characteristics. Additionally, the proposed strategy ensures robust control even in the presence of faults in current sensors. Simulation results demonstrate the superiority of the proposed method compared to recent approaches, and experimental results confirm its viability.

ARTICLE HISTORY
Received 4 March 2024
Accepted 8 November 2024

1. Introduction

The permanent magnet synchronous machine (PMSM) has garnered increased attention in recent years [1] for use in electromechanical energy conversion systems (ENCSs), whether based on fossil fuels or renewable sources [2]. It is also applicable in energy storage systems [3]. Compared to other types, such as single- or doubly-fed induction machines [4], the PMSM offers a higher power-to-weight ratio and eliminates the need for a gearbox.

A PMSM-based electromechanical energy conversion system (ENCS) can operate as a stand-alone system [5] or be connected to a power grid [6]. The utilization of a PMSM within an ENCS varies depending on the control configuration of the machine (generator). Two main configurations are identified: the first is based on active power control, and the second is based on speed control [7]. In both configurations, the reference for the direct component of the current is set to zero. This approach is intended to expand the range of electromagnetic torque variation, which is directly related to the q-axis component of the current, and to minimize losses. The speed control configuration is often preferred due to its relative simplicity compared to the active power control configuration, where the control output directly depends on the control inputs. Additionally, the speed control configuration is more commonly used for PMSM-based energy storage systems.

Recent control approaches have been proposed to enhance the speed control performance of PMSMs. One method, developed in [8], utilizes an H-Infinity strategy for both speed control and mechanical load estimation. This approach incorporates a feedforward term for accurate tracking but relies on the knowledge of machine parameters and involves complex calculations through linear matrix inequality (LMI) resolution. Another linear control method, synthesized in the frequency domain, is discussed in ref. [9]. The performance of this method depends on real-time estimates of system parameters. Both methods share a common weakness: sensitivity to non-modeled dynamics.

To address this issue, ref. [10] introduced an adaptive PID controller with variable structure terms. This method does not use the inner current control loop; however, it calculates some control law parameters based on integral and derivative functions, which increases sensitivity to measurement noise and offsets. Additionally, this approach requires a higher implementation frequency.

The works in [11] and [12] focused on synthesizing nonlinear surface-based sliding mode control for the speed control of permanent magnet Vernier machines (which have a similar model to classical PMSMs). However, these approaches require knowledge of mechanical quantities and are dependent on the precision of speed sensors, as they rely on accurate control error dynamics.

The authors in refs [13,14] developed adaptive feedback linearization control strategies. These algorithms are designed for estimating non-modeled electrical quantities, such as mechanical torque and parameter variations. However, this approach is effective primarily

CONTACT Abdelhak Djoudi abdelhak.djoudi@hotmail.com CDER, Centre de Développement des Energies Renouvelables, Route de l'Observatoire Bouzeréah, Algiers, Algeria

for low-frequency electrical quantities and requires a higher computational burden and control frequency to ensure convergence.

In ref. [15], the authors proposed a linear/nonlinear switching control with active disturbance rejection. A variable structure function was employed to ensure robustness. The disturbance function includes unmodeled quantities. This method requires solving differential equations for its implementation, which may necessitate a high control frequency. However, this frequency is limited by the switching of one of the stator-side converters. In ref. [16], an adaptive backstepping speed control was developed for a surface-mounted PMSG, which is valid for systems with unknown parameters. However, this method is sensitive to unmodeled dynamics and requires solving an online optimization problem.

Predictive methods have also been applied to speed control. They can be categorized into two main types: direct and indirect. The direct method is based on a single control loop [17–20], primarily focused on controlling the rotating speed. Additionally, it ensures objectives such as the maximum torque per ampere (MTPA) strategy. The states of the stator-side converter switches are determined by solving a fitness function, which is calculated and updated according to the control frequency. The fitness function is evaluated based on the models of the PMSG and the stator-side converter. It should be noted that with this method, the dynamics of the q-axis current component are not controlled, which can result in undesirable behaviour, such as current fluctuations, especially in systems with high inertia. This can lead to increased converter and machine losses, ultimately reducing the system's lifetime.

The category of indirect control methods overcomes these drawbacks by employing cascaded control loops. The inner control loop is responsible for controlling the current components, with several methods specifically designed for this purpose. The outer control loop manages the rotating speed by determining the required q-axis current reference. In ref. [21], the authors proposed a predictive-based deadbeat speed control, where the command output is the reference for the q-axis current component. The inner control loop also uses predictive control to select the optimal switch states based on a fitness function for current control. However, this method remains sensitive to parameter variations because it directly depends on the machine model. The control strategy developed in ref. [22] addresses this issue by implementing an adaptive approach with the estimation of unknown quantities. This approach is based on ultra-local model control for both control loops, but it is still sensitive to machine demagnetization. It is also noted that in predictive control methods, the prediction of the machine state relies on the Euler discretization method, which is susceptible to noise and inaccuracies due to the limited fidelity of the sensors.

A flatness theory-based approach for PMSG control loops was elaborated in ref. [23]. However, this method does not ensure robustness to parameter variations, as verified by the Lyapunov criteria. In ref. [24], the authors proposed a direct control law based on an adaptive linear function, where the gains are optimized through a genetic algorithm. Unfortunately, these gains are obtained using a simplified PMSM model that only applies to a specific operating point and set of machine parameters. As a result, the stability at other operating points or with different machine parameters is not guaranteed, and the dynamic behaviour of the currents is not controlled.

Cascaded sliding mode methods have been proposed as a viable alternative for controlling the behaviour of speed and current components. In refs. [25,26], an adaptive sliding mode controller was synthesized to reduce the gain, which is directly related to the chattering phenomenon. Specifically, the unmodeled quantity described by the mechanical equation is estimated and injected into the classical sliding mode controller. In ref. [26], the gain is set as a proportional function of the tracking error, which can lead to undesirable behaviour of the speed near the reference value. In ref. [27], an adaptive sliding mode control based on the saturation function was proposed, but this approach results in decreased performance compared to the sign function-based method. Additionally, this direct method does not control the current behaviour effectively.

The control law proposed in this paper offers enhanced properties compared to the previously mentioned methods. It utilizes cascaded control to effectively manage current behaviour, with a particular focus on the outer control loop for speed. This approach is based on simple formulas, leading to reduced computational burden and increased reliability. Unlike methods previously proposed in the literature, our approach does not require an online estimation algorithm for the unmodeled quantities related to mechanical behaviour. This makes it robust even in the presence of imperfections in the inner control loop.

The rest of the paper is organized into five main sections. The first section provides a brief description of the problem statement. The second section presents a simplified model of the machine. The third section details the developed control approach. The fourth section demonstrates the superiority of the proposed method compared to a recent one published in the literature, using simulation results. Finally, the fifth and sixth sections are dedicated to experimental validation and the conclusion, respectively.

2. Problem statement

The operation of the controlled PMSM-based entrainment system is depicted in Figure 1. The PMSM

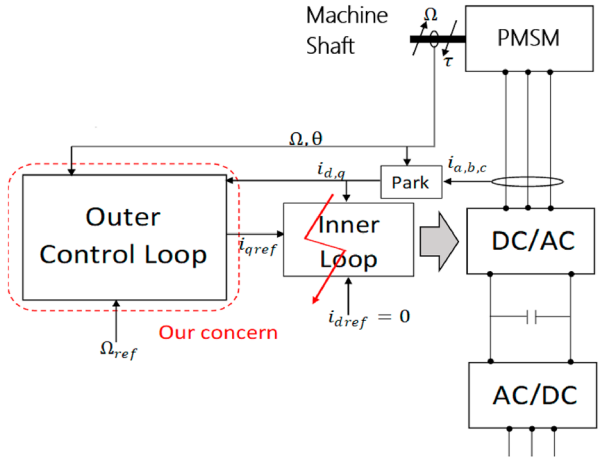

Figure 1. Controlled PMSM-based entrainment system.

converts mechanical power, characterized by torque τ and rotating speed Ω, to electrical power or vice versa. The electrical currents are sinusoidal, and the voltages applied to the generator terminals are generated through a stator-side converter. The system controls the rotating speed and the d-axis current component i_d. The reference for the rotating speed is Ω_{ref}, while the reference for the d-axis current component i_{dref} is set to zero.

Cascaded speed control consists of two main loops. The outer loop, which is the focus of this paper, is responsible for determining the q-axis current reference i_{qref}. The inner control loop manages the behaviour of the dq-axis generator currents (i_d, i_q). These currents are derived from the Park transformation of the three-phase currents $i_{a,b,c}$. The goal of this paper is to develop an outer loop control that is independent of PMSM parameters, making it insensitive to parameter variations. This approach avoids the use of a torque estimation algorithm, thereby increasing reliability and reducing computational burden. Additionally, it ensures control effectiveness even in the presence of current sensor offset faults.

3. PMSM model

dq synchronous reference frame model of three-phase PMSM is given by system Equations (1).

$$\begin{cases} \dfrac{di_d}{dt} = -\dfrac{R_s}{L_d} i_d + \omega_s \dfrac{L_q}{L_d} i_q + \dfrac{1}{L_d} u_d \\ \dfrac{di_q}{dt} = -\dfrac{R_s}{L_q} i_q - \omega_s \dfrac{L_d}{L_q} i_d - \dfrac{\lambda_m}{L_q} \omega_s + \dfrac{1}{L_q} u_q \\ J\dfrac{d\Omega}{dt} = C_{em} + \tau - C_f, \omega_s = p\Omega \\ C_{em} = \dfrac{3}{2} p(\lambda_m i_q + (L_d - L_q) i_d i_q) \\ C_f = \mu \Omega \end{cases} \quad (1)$$

The inputs of PMSM are as follows

Table 1. PMSM parameters designation.

Parameter	Designation
R_s	stator resistance
L_d	d-axis inductance
L_q	q-axis inductance
λ_m	flux linkage
J	system inertia
ω_s	electrical pulsation (Turbine and PMSG)

u_d, u_q are dq components of stator voltages. τ represents the mechanical torque.

The internal states of the system:

i_d, i_q are dq components of stator currents. C_{em} is the electromagnetic torque. C_f represents the friction torque. d- and q-component (φ_d, φ_q) of stator flux linkage vector are given by system Equation (2) as

$$\begin{cases} \varphi_d = L_d i_d + \lambda_m \\ \varphi_q = L_q i_q \end{cases} \quad (2)$$

The outputs are the speed Ω and d-axis component of the current i_d.

The parameters of the system are given in Table 1.

4. Elaboration of the proposed method

The purpose of this section is to synthesize a control law for the outer loop with the characteristics described in the previous section. The proposed control law is outlined as follows:

$$i_{qref} = \frac{\alpha}{s+\beta} \text{sign}(\Delta\Omega) + i_{ql} \quad (3)$$

where α and β are positive coefficients.

Considering the calculation frequencies, let f_Ω be the frequency for the term $(\text{sign}(\Delta\Omega))$ and f_d be the frequency for the term $\left(\frac{\alpha}{s+\beta}\right)$, where s is the Laplace operator. The tracking error $\Delta\Omega$ is defined as follows:

$$\Delta\Omega = \Omega_{ref} - \Omega \quad (4)$$

The dynamic of the speed is as given in (5).

$$\frac{d\Omega}{dt} = \frac{3}{2}\frac{p\lambda_m}{J} i_q + \frac{3}{2}\frac{p}{J}(L_d - L_q) i_d i_q + \frac{p}{J}(\tau - C_f) \quad (5)$$

Or,

$$\frac{d\Omega}{dt} = a i_q + b i_d i_q + c\tau_t \quad (6)$$

where

$$a = \frac{3}{2}\frac{p\lambda_m}{J}, b = \frac{3}{2}\frac{p}{J}(L_d - L_q), c = \frac{p}{J} \quad (7)$$

$$\tau_t = \tau - C_f \quad (8)$$

Considering the tracking errors of dq currents components like Δi_d, Δi_q, respectively. The latter are given by relation (9).

$$\begin{cases} \Delta i_d = i_{dref} - i_d \\ \Delta i_q = i_{qref} - i_q \end{cases} \quad (9)$$

The speed dynamic error is written in function of Δi_d and Δi_q as follows.

$$\frac{d(\Delta\Omega)}{dt} = a i_{qref} + c\tau_t + \Delta - \frac{d\Omega_{ref}}{dt} \tag{10}$$

The quantity Δ_I is defined in (11) where d-axis current component reference is set to be null.

$$\Delta = -a\Delta i_q + b\Delta i_d \Delta i_q - b i_{qref}\Delta i_d \tag{11}$$

The speed reference is given as steps which are referred by the intervals $N_i = [t_i, t_i + T_{sr}[\,, i = 1, 2\ldots$ and $t_i + T_{sr} = t_{i+1}$. So, for time instant $t \in$ to a given N_i, relation (11) becomes:

$$\frac{d(\Delta\Omega)}{dt} = a i_{qref} + c\tau_t + \Delta \tag{12}$$

Replacing the quantity (3) in relation (12), the dynamic of the tracking speed error is given by (13).

$$\frac{d(\Delta\Omega)}{dt} = \frac{a\alpha}{s+\beta}\text{sign}(\Delta\Omega) + c\tau_t + \Delta_I \tag{13}$$

where

$$\Delta_I = \Delta + i_{ql} \tag{14}$$

Inserting a low pass filter for both parts of the last equation. The filter model $F(s)$ is given by relation (15).

$$F(s) = \frac{1}{\sigma s + 1} \tag{15}$$

The coefficient σ set the dynamic of the filter. This filter needed to filter high frequency part. Relation (13) becomes

$$(\Delta\Omega)_F(s) = \frac{a\alpha}{(s+\beta)(\sigma s+1)}\text{sign}(\Delta\Omega) + c\tau_{tF} + \Delta_{IF} \tag{16}$$

where $\Delta_{IF}, \tau_{tF}, i_{qrefF}, (\Delta\Omega)_F$ are filtered quantities of $\Delta_I, \tau_t, i_{qref}, \Delta\Omega$, respectively, in the Laplace domain. PMSG parameters variations are practically null and neglected during that interval.

Taking into account, the dynamics of Ω, τ_t, i_{qref} are very slow compared to that of the filter F, therefore:

$$\Omega = {\Omega_F}^t, \tau_t = {\tau_{tF}}^t, i_{qref} = {i_{qrefF}}^t \tag{17}$$

${\Omega_F}^t, {\tau_{tF}}^t, {i_{qrefF}}^t$ standing for $\Omega_F, \tau_{tF}, i_{qrefF}$ in time domain.

The latter relation is ensured if the coefficient σ verifies the following condition:

$$0 < \sigma \ll \left(\frac{1}{J}, \frac{1}{\beta}\right) \tag{17.1}$$

Relation (16) becomes as given by (18) in time domain.

$$\frac{d(\Delta\Omega)}{dt} = \left(\frac{a\alpha}{(s+\beta)(\sigma s+1)}\right)_t \text{sign}(\Delta\Omega) + c\tau_t + {\Delta_{IF}}^t \tag{18}$$

${\Delta_{IF}}^t$ and $\left(\frac{a\alpha}{(s+\beta)(\sigma s+1)}\right)_t$ standing, respectively, for $\Delta_{IF}, \left(\frac{a\alpha}{(s+\beta)(\sigma s+1)}\right)$ in time domain.

That implies relation (19).

$$\frac{d^2(\Delta\Omega)}{dt^2} + \beta\frac{d(\Delta\Omega)}{dt} = \left(\frac{a\alpha}{(\sigma s+1)}\right)_t \text{sign}(\Delta\Omega) + c\beta\tau_t + \beta{\Delta_{IF}}^t + c\dot{\tau}_t + {\Delta_{IF}}^{\cdot t} \tag{19}$$

$\left(\frac{a\alpha}{(\sigma s+1)}\right)_t$ standing for $\left(\frac{a\alpha}{(\sigma s+1)}\right)$ in time domain.

Knowing that the quantities $\frac{d^k(\Delta\Omega)}{dt^k}, k = 2, 3, \ddot{\tau}_t$ are neglected, and $\sigma \ll 1$, so relation (19) tends to the following form:

$$\frac{d(\Delta\Omega)}{dt} = \frac{a\alpha}{\beta}\text{sign}(\Delta\Omega) + \frac{c\beta\tau_t + \beta{\Delta_{IF}}^t + c\dot{\tau}_t + {\Delta_{IF}}^{\cdot t}}{\beta} \tag{19.1}$$

Considering the control parameter α is negative. Relation (19.1) rewritten as in (20).

$$\frac{d(\Delta\Omega)}{dt} = -|(a\alpha)/\beta|\text{sign}(\Delta\Omega) + \frac{c\beta\tau_t + \beta{\Delta_{IF}}^t + c\dot{\tau}_t + {\Delta_{IF}}^{\cdot t}}{\beta} \tag{20}$$

Taking the Lyapunov function V defined as:

$$V = \frac{1}{2}(\Delta\Omega)^2 \tag{21}$$

Its derivative time $\dot{V}$ expressed as follows:

$$\dot{V} = -|(a\alpha)/\beta||\Delta\Omega| + \frac{c\beta\tau_t + \beta{\Delta_{IF}}^t + c\dot{\tau}_t + {\dot{\Delta}_{IF}}^t}{\beta}(\Delta\Omega) \tag{22}$$

The convergence of V to zero is ensured if:

$$\dot{V} < 0 \tag{23}$$

That relation is verified in the case when the regulator parameter α selected as:

$$|\alpha| > \frac{1}{a}|c\beta\tau_t + \beta{\Delta_{IF}}^t + c\dot{\tau}_t + {\dot{\Delta}_{IF}}^t| \tag{24}$$

For that case:

$$(V, \Omega) \overset{\text{converge to}}{\rightarrow} (0, \Omega_{ref}) \tag{25}$$

Let's find an accurate convergence condition about the parameter α. This all using relations (3) and (24) and taking into account the operating limit of stator current.

Taking into account the tolerated rate of q-axis component current given by I_{qmax}. Therefore:

$$|i_{qref}| = \left|\left(\frac{\alpha}{s+\beta}\right)_t \text{sign}(\Delta\Omega) + i_{ql}\right| \leq I_{qmax} \tag{26}$$

$\left(\frac{\alpha}{s+\beta}\right)_t$ stands for $\left(\frac{\alpha}{s+\beta}\right)$ in time domain.

The last is ensured once:

$$\left|\frac{\alpha}{\beta}\right| + \max(|i_{ql}|) \leq I_{qmax} \tag{27}$$

That found after taking into accountthe function i_{qref} is monotone during a given period calculating time $\frac{1}{f_\Omega}$. The maximum value is calculated for steady-state response to unit step considering Laplace transferfunction $\frac{\alpha}{s+\beta}$.

It is resumed that the convergence condition of the proposed control law related to the parameter $|\alpha|$ as:

$$M < |\alpha| < \beta I_{qmax} \tag{28}$$

where

$$M = \frac{1}{a}|c\beta\tau_t + \beta\Delta_{IF}{}^t + c\dot{\tau}_t + \dot{\Delta}_{IF}{}^t| \tag{29}$$

The last relation is simplified taking into account the specifications of $\tau_t, \dot{\tau}_t, \Delta_{IF}, \dot{\Delta}_{IF}$. It is noticed that:$M$ is bounded by the term ϑ and.

$$\vartheta = \frac{1}{a}\text{Max}(c\beta\tau_t + \beta\Delta_{IF}{}^t + c\dot{\tau}_t + \dot{\Delta}_{IF}{}^t) \tag{30}$$

The term $c\dot{\tau}_t + \dot{\Delta}_{IF}^t$ is given by relation (31).

$$c\dot{\tau}_t + \dot{\Delta}_{IF}^t = \frac{d^2(\Delta\Omega)}{dt^2} - a\alpha\frac{d\left(\frac{1}{s+\beta}\text{sign}(\Delta\Omega)\right)_t}{dt} \tag{31}$$

where $\left(\frac{1}{s+\beta}\text{sign}(\Delta\Omega)\right)_t$ stand for $\left(\frac{1}{s+\beta}\text{sign}(\Delta\Omega)\right)$ in the time domain.

And:

$$\left|\frac{d\left(\frac{1}{s+\beta}\text{sign}(\Delta\Omega)\right)_t}{dt}\right| \leq 2 \tag{32}$$

In one hand, $\frac{d^2(\Delta\Omega)}{dt^2}$ is neglected. The term $c\dot{\tau}_t + \dot{\Delta}_{IF}^t$ is given as in (32). In other side, the quantity $\Delta_{IF}{}^t$ is given in relation (33).

$$\Delta_{IF}{}^t = -a\Delta i_{qF} + (b\Delta i_d\Delta i_q - bi_{qref}\Delta i_d) + ai_{qlF} \tag{33}$$

where $\Delta i_{qF}, i_{qlF}$ are the filtered quantity of $\Delta i_q, i_{ql}$ through the filter F in time domain.

The term $(b\Delta i_d\Delta i_q - bi_{qref}\Delta i_d)$ is neglected, and:

$$\Delta_{IF}{}^t = -a\Delta i_{qF} + i_{qlF} \tag{34}$$

Δ_{IF} is bounded as follows:

$$|\Delta_{IF}{}^t| < a\Delta I_m + \max(|i_{ql}|) \tag{35}$$

where ΔI_m is the absolute value of maximum tolerated q-axis component current tracking error.

Taking into account (34) and (35), (28) becomes.

$$\frac{1}{a}\text{Max}(c\beta\tau_t + a\beta(i_{qlF}) + \beta(-a\Delta i_{qF}) + 2a\alpha) < |\alpha| < \beta I_{qmax} \tag{36}$$

The convergence condition of the controlled system is verified if:

$$abs\left(i_{ql} + \frac{c}{a}\tau_t + 2\alpha\left(\frac{1}{\beta}\right)\right) + \Delta I_m < \frac{|\alpha|}{\beta} < I_{qmax} \tag{37}$$

Setting

$$\bar{M} = \beta abs\left(i_{ql} + \frac{c}{a}\tau_t + 2\alpha\left(\frac{1}{\beta}\right)\right) + \beta\Delta I_m \tag{38}$$

4.1. Finite-time convergence

This subsection is dedicated to know more about the convergence time of the concerned control loop.

From relations (20) and (36), it is concluded about the behaviour of speed dynamic that:

$$-\partial\text{sign}(\Delta\Omega) - \beta a\bar{M} < \frac{d(\Delta\Omega)}{dt} < -\partial\text{sign}(\Delta\Omega) + \beta a\bar{M} \tag{39}$$

where $\partial = |(a\alpha)/\beta|$.

For the case when $\Delta\Omega(t_i) > 0$ the tracking control error is bounded as given by (38).

$$-(\partial + \beta a\bar{M})(t - t_i) < \Delta\Omega|_{t_i}^t < -(\partial - \beta a\bar{M})(t - t_i) \tag{40}$$

where t is a time variable. $t \in N_i$. (39) is written as in (40).

$$-\emptyset_M < t + \Delta\Omega(t_i) < \Delta\Omega(t) < -\emptyset_m < t + \Delta\Omega(t_i) \tag{41}$$

where.

$$\emptyset_M = (\partial + \beta a\bar{M}), \emptyset_m = (\partial - \beta a\bar{M}), \Delta t = (t - t_i)$$

The convergence time t_c is concluded from (41) taking purpose $\Delta\Omega(t) = 0$. So:

$$\frac{\Delta\Omega(t_i)}{\emptyset_M} < t_c < \frac{\Delta\Omega(t_i)}{\emptyset_m} \tag{41.1}$$

For the case when $\Delta\Omega < 0$, the tracking error is bounded as in (42).

$$\emptyset_m(t - t_i) < \Delta\Omega|_{t_i}^t < \emptyset_M(t - t_i) \tag{42}$$

The convergence time given in (43).

$$-\frac{\Delta\Omega(t_i)}{\emptyset_M} < t_c < -\frac{\Delta\Omega(t_i)}{\emptyset_m} \tag{43}$$

Convergence time for both last cases is generalized by relation (44).

$$\frac{|\Delta\Omega(t_i)|}{\emptyset_M} < t_c < \frac{|\Delta\Omega(t_i)|}{\emptyset_m} \tag{44}$$

4.2. Choice of f_Ω, f_d and T_{sr}

The calculating frequency f_Ω related to outer control loop is chosen to be less than the convergence time of the innercontrol loop. Updating time of speed reference T_{sr} is chosen in such way to be bigger than convergence time of the outer control loop t_c. The calculating frequency f_d of the term $\left(\frac{\alpha}{s+\beta}\right)$ is set to be very bigger than the time constant $\frac{\alpha}{\beta}$. The last quantity is the convergence time of the quantity $\left(\frac{\alpha}{s+\beta}\right)$.

4.3. Overall consequence

The outer loop, defined by the control law (3), allows for speed control if the control parameters satisfy the condition given in relation (37). These parameters do not depend on the knowledge of the mechanical characteristics of the turbine. This method remains effective even in the presence of q-axis current offset errors in the inner control loop. It does not require estimation of mechanical torque, magnetic flux or inertia, relying instead on simple formulas. The method is characterized by finite-time convergence, as indicated by relation (44). Notably, the proposed control law does not rely solely on current measurements, making it robust against current sensor faults. The block diagram of the proposed method is illustrated in Figure 2.

5. Simulations results based comparative study

The effectiveness of the proposed method is compared to a latest method published in the literature [26] (Method I) through simulations. The parameters of the considered machine are given in Table 2. The parameters of the developed control method are set to be $\alpha = 1000, \beta = 40$. The adaptive gain f_w for method II is given by relation (45). All mechanical parameters are set to be known for method I. For method II, these quantities are assumed unknown.

$$f_w = 200|\Delta\Omega|(1.5 - 0.01e^{(-10|\Delta\Omega|)}) \qquad (45)$$

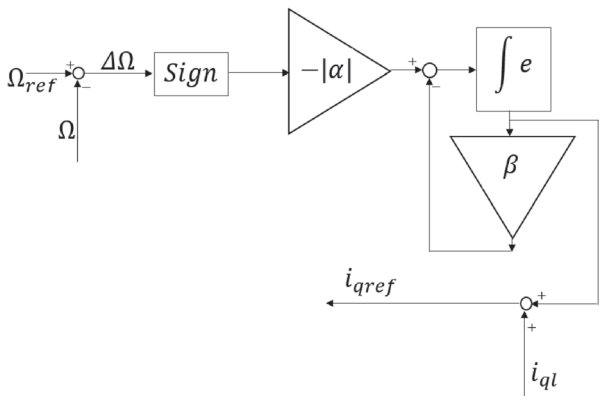

Figure 2. Block diagram of the proposed control law.

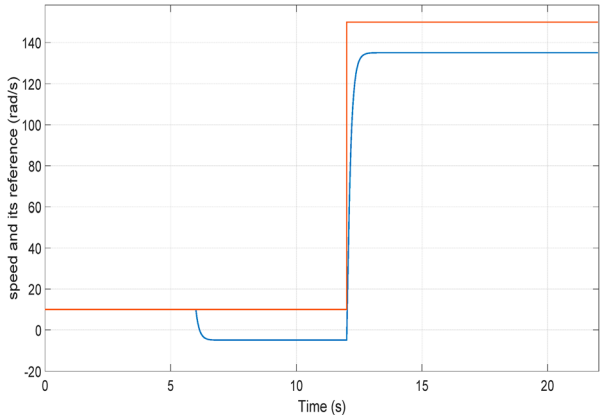

Figure 3. Rotating speed and its reference (method I).

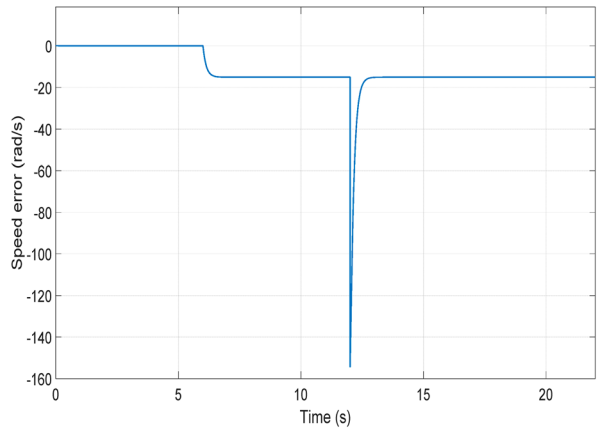

Figure 4. Error of speed control (method I).

Table 2. PMSG characteristics.

Number of pole pairs	4
Nominal stator phase resistance	0.1Ω
Nominal d-axis inductance	0.85 mH
Nominal q-axis inductance	0.95 mH
Nominal magnet flux	0.1 Wb
Maximum current	25 A
Inertia	0.01 Kg.m^2
Nominal power	5000 Watt

The simulations were conducted using MATLAB/SIMULINK and are based on a small-signal model of the PMSM. The external torque is taken to be equal to 2 N.m for the first 6 s. It is equal to 8 N.m for the last time interval. A sensor offset of 3 A is introduced at the time $t = 6$ s in order to simulate sensors currents default. The magnet flux is stepped to take 250% of the nominal one at the time $t = 6$ s. For the time interval $[0, 6\,\text{s}]$, the magnet flux is considered equal to its nominal value. The quantity i_{ql} is artificially limited to 22 A by applying a q-axis current limiter. The simulation results are given in Figures 3–5 for method I and in Figures 6–10 for the proposed method (method II).

It is remarked that during the time interval $[0, 6\,\text{s}[$, the speed tracking the reference (10 rad/s) for the case of methods I and II (Figures 3,4,6,8 and 9, respectively). The tracking error remains negligible compared

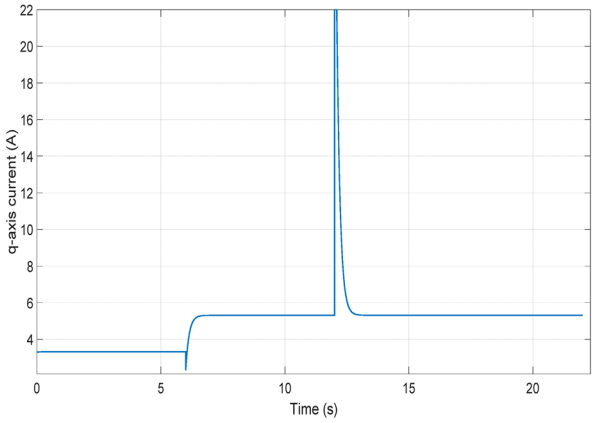

Figure 5. q-axis current (method I).

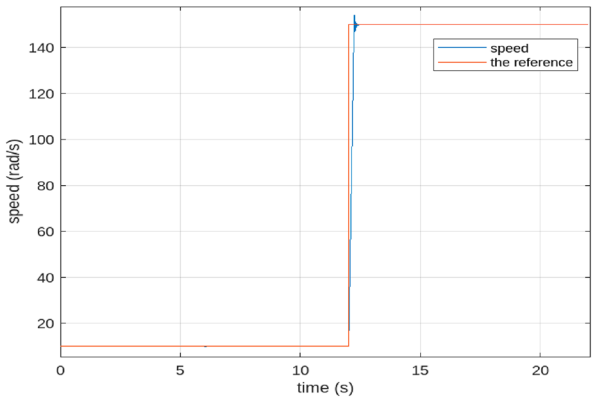

Figure 6. Speed and its reference (method II).

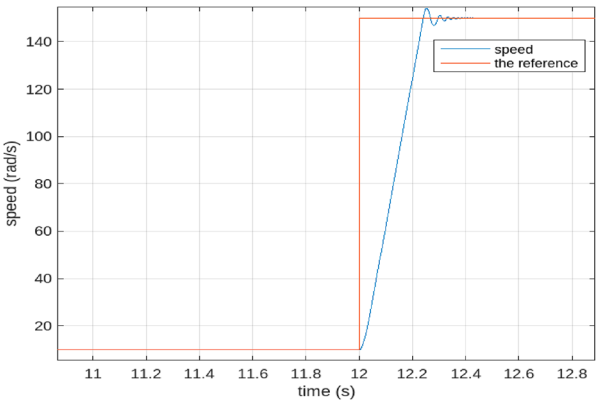

Figure 7. Zoom of speed and its reference (method II).

to the reference speed. The q-axis current component is around 3.34 A (Figure 5).

During the time interval [6 s, 12 s[, the speed control related to the method I is not ensured where the control error is 16.4 rad/s, which represents more than 160% of the reference speed (Figures 3,4,6,7 and 9, respectively).

The speed control target related to the proposed method is ensured and the control error is 1%. The steady state of the q-axis current is 5.35 A, which remains tolerable (Figures 5 and 10, respectively).

For the interval time [6 s, 12 s[, the speed reference stepped to 150 rad/s. The convergence of the control target is not ensured for the method I where the

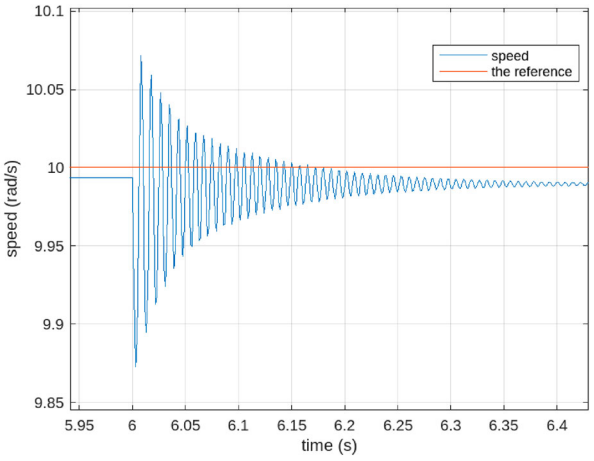

Figure 8. Zoom of speed and its reference (method II).

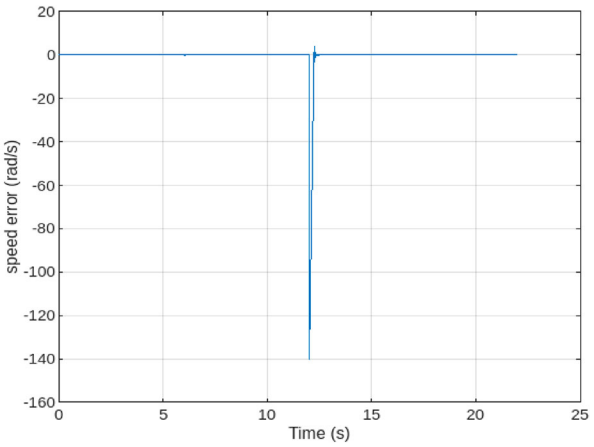

Figure 9. Error of speed control (method II).

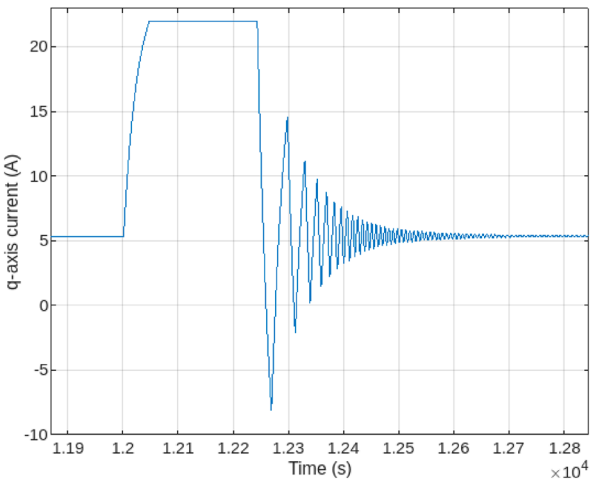

Figure 10. q-axis current component (method II).

steady-state error is 16.4 rad/s which is more than 10% compared to the reference one (Figures 3,4,6,8 and 9, respectively). The proposed method (II) allows for accurate tracking even in the presence of current sensor faults and without requiring knowledge of mechanical quantities. The q-axis current component stills bounded as required (Figure 10). The response time of method II is 0.24 s.

As consequence, the proposed method offers better performances compared to method I.

6. Experimental validation

The viability of the developed control method is highlighted via experimental validation, which was done on the PMSM-based test bench. The characteristics of the machine are given in Table 2.

6.1. Test bench description

The test bench is shown in Figure 11. It is composed of three parts. The first one (Figure 11(A)) gathers PMSM, which is the target machine and the DC one used to generate mechanical power, which is transmitted to the generator by the rotor shaft. The cited machines are mechanically coupled. The DC machine is used to emulate a hydropower turbine like Semi-Kaplan one. It generates a reference torque which is the function of rotor speed. This part incorporates an encoder, which permits measuring the rotor position and rotating speed. The second part (Figure 11(B)) contains the necessary equipment allowing the control of the DC machine and the PMSM. The last allows commanding the rotor speed through two cascaded loops. The inner one is utilized to control the rotor currents. That equipment is mainly a set of power electronics converters, passive filters, AC/DC currents and voltage sensors, and transformers. The test bench is utilized through real simulation assisted by computers. PMSM driving is ensured via the dSPACE system and Matlab/SIMULINK. The DC machine driving is based on another calculator system and soft means. The last is considered as the third part of the test bench.

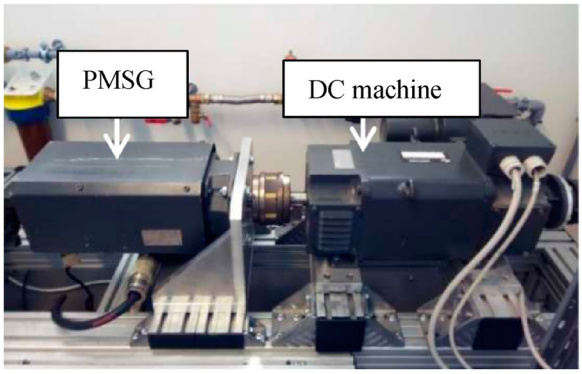

(A)

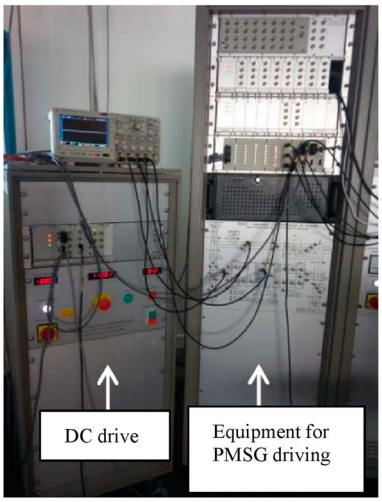

(B)

Figure 11. Components of the benchmark.

6.2. Experimental results

Experimental results given in this paper stand for the speed control method given in relation (3), which is schematized by Figure 2. The parameters of the applied control law are given as:

$$f_d = 10^4\text{Hz}, f_\Omega = 10^4\text{Hz}, \sigma = 10^{-3}, \alpha = 20, \beta = 10 \tag{45}$$

The value of i_{ql} is taken as equal to measured q-axis current i_q with maximum value equal to 20 A. The profile of the speed reference is given under three phases. Phase I corresponding to the reference $\Omega_{ref} = 100$ rad/s. It is given during the time interval $[0, 10.8[$ s. Phase II corresponding to the reference $\Omega_{ref} = 153$ rad/s. It is given during the time interval $[10.8, 27.5[$ s. Phase III corresponding to the reference $\Omega_{ref} = 126$ rad/s. It is given during the time interval $[27.5, 40[$ s.

The response of PMSM under safe currents sensors is given through Figures 12–14. Figure 12(A) depict measured speed and different related references. During phase I, the speed tracking its reference with error inferior than 5 rad/s. This last present 5% compared to the controlled speed.q-current amplitude corresponding to this phase is around −20.3 rad/s. When the speed reference changes with step mannerto 153 rad/s(under phase II), the real speed takes around 1.1 s to reach its reference. After that transient regime where q-axis component current remain evolving within acceptable bound; in the steady-state corresponding to phase II, the tracking speed error remain less than 4 rad/s. The last present around 2.5% of the rotor speed.

The value of the q-axis component current takes around −9.7 A. For the case of phase III, two regimes are distinguished. The first one is the transient regime corresponding while stepping the speed reference from 153 rad/s to 126 rad/s. The real speed takes around 0.9 s to achieve its reference while keeping the response of q-axis component current within acceptable bound. The second regime is the steady-state where the tracking

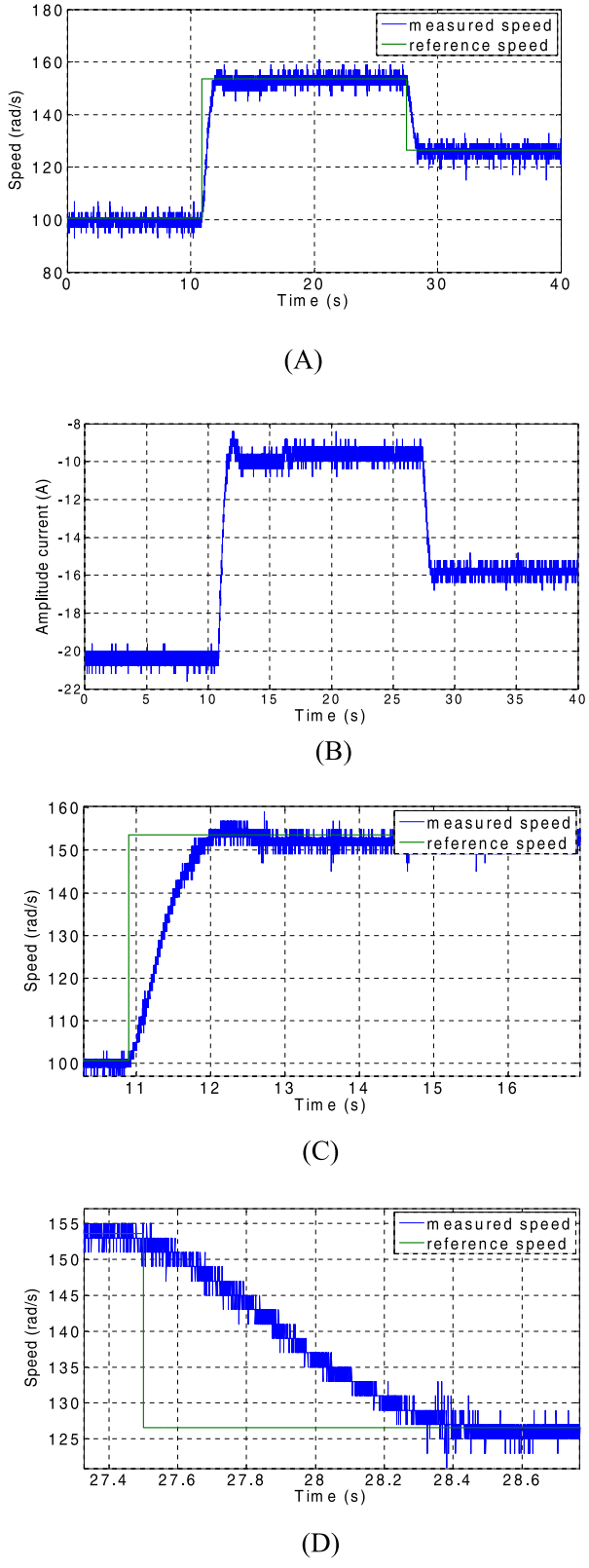

Figure 12. PMSG response. (A) Profile of speed and its reference. (B) Stator current amplitude profile. (C) and (D) Zoom of (A).

error is less than 2.25% compared to the real measured speed. This last corresponds is less than 3 rad/s.

Figures 13–15 show the behaviour of the generator under steady-state while controlling the rotor speed. That regime was reproduced by experimental for the

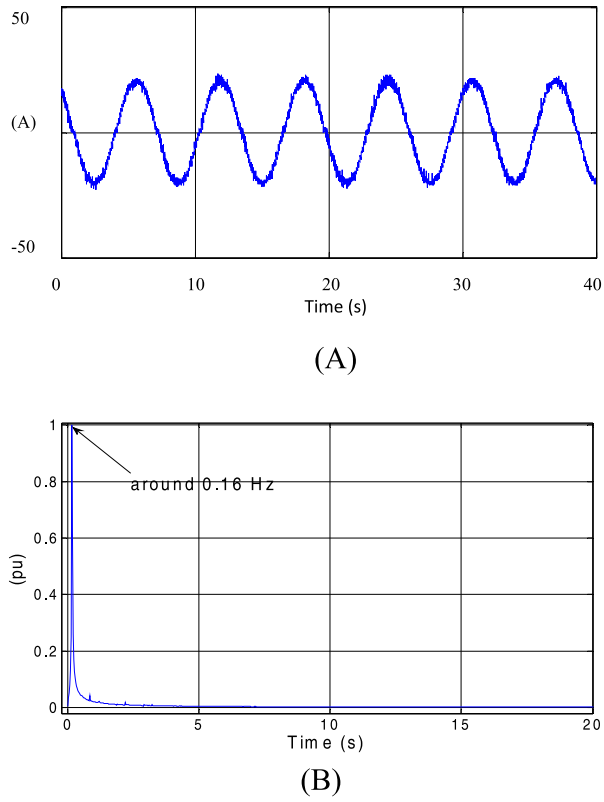

Figure 13. Stator currents characteristics in steady-state during phase I. (A) Waveform of one phase current. (B) Appeared frequencies.

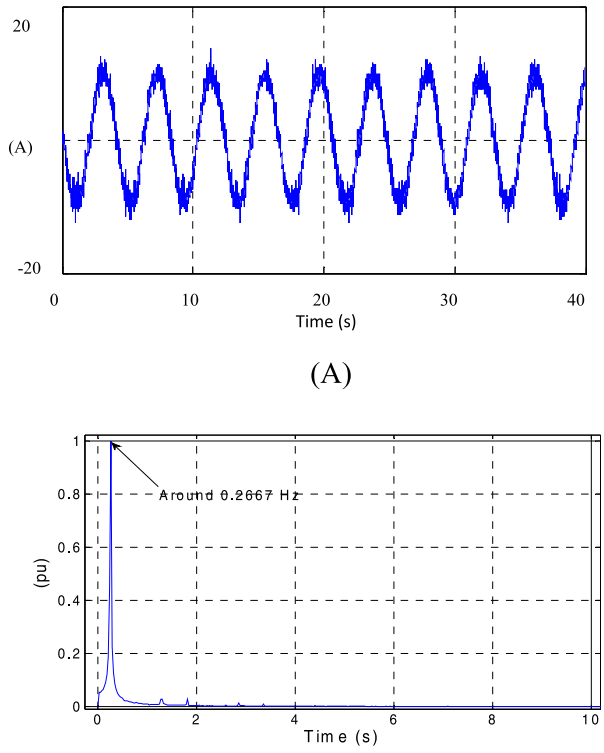

Figure 14. Stator currents characteristics in steady-state during phase II. (A) Waveform of one phase current. (B) Appeared frequencies.

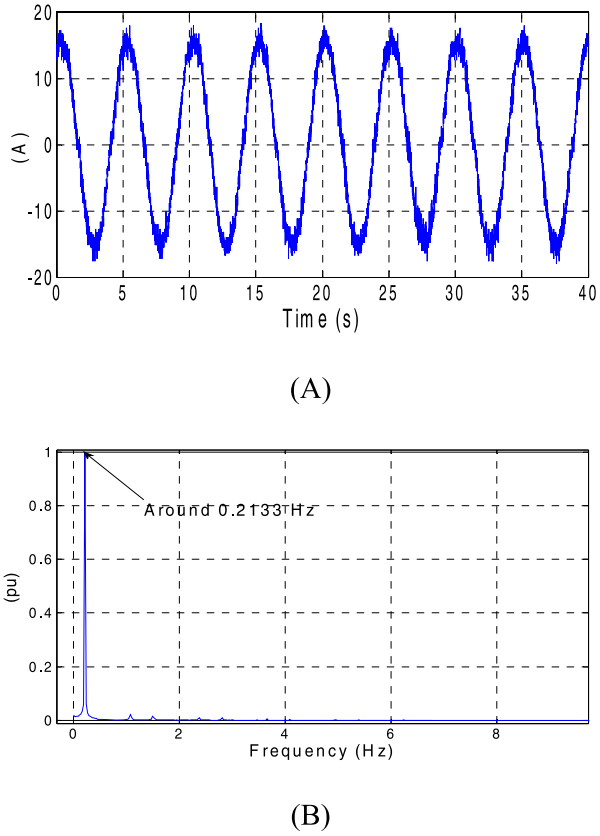

Figure 15. Stator currents characteristics in steady-state during phase III. (A) Waveform of one phase current. (B) Appeared frequencies.

reference as given in phase I. The waveform of one phase current is given in Figure 13(A). Its frequency spectrum is given in Figure 13(B). The correspondent total harmonic distortion (THD) is 3.9%. The main frequency is 0.16 Hz.

The profile of one phase current while reproducing the regime of steady-state under phase II or when the reference speed is set to 153 rad/s is given in Figure 14(A). Frequencies spectrum linked to that profile is as given in Figure 14(B). The THD takes the value 4.9%. The main frequency is 0.2667 Hz.

The experimental results relative when reproducing the regime of steady-state under phase III are given in Figure 15(A,B). Figure 15(A) represents the waveform of one phase current. Its THD is 4.8% and its frequencies spectrum is given by Figure 15(B). The main frequency is 0.2133 Hz.

Regarding to the experimental results dedicated by Figures 12–15 in order to validate the efficiency of the proposed speed control method,which does not require the knowledge of mechanical characteristics of the target system, the presented one is then verified.

7. Conclusion

This paper presents a novel approach to speed control for a permanent magnet synchronous machine (PMSM), focusing on overcoming the challenges associated with current harmonics and overcurrent demands. Unlike existing methods, which often rely on complex online algorithms for torque and magnetic flux estimation, the proposed strategy offers simplicity and robustness by being independent of these parameters, including system inertia. The method's resilience to unmodeled quantities is rigorously demonstrated through stability proofs, ensuring reliable performance even in the presence of sensor offsets. The practical effectiveness of this approach is validated through real-time simulations using the dSPACE system, where the PMSM is coupled with a mechanically emulated turbine via a DC machine. The results, confirmed through a comparative study, clearly indicate that the proposed control strategy not only meets but exceeds the performance benchmarks set by recent methods in the literature. This work contributes a significant advancement in PMSM control by providing a robust, simple and efficient solution to a complex problem. The proposed control strategy for PMSMs offers significant potential across various systems.

Disclosure statement

No potential conflict of interest was reported by the author(s).

References

[1] Yee Heng T, Jian Ding T, Choe Wei Chang C, et al. Permanent magnet synchronous generator design optimization for wind energy conversion system: A review. Energy Rep. 2022;8:277–282. doi:10.1016/j.egyr.2022.10.239

[2] Siddique MA, Nobanee H, Hasan MB, et al. How do energy markets react to climate policy uncertainty? Fossil vs. renewable and low-carbon energy assets. Energy Econ. 2023;128:107195. doi:10.1016/j.eneco.2023.107195

[3] Taraft S, Rekioua D, Djoudi A, et al. Reference power point tracking reference power point tracking of the inertial storage system connected to the electrical grid. Math Model Eng Probl. 2024;11(5).

[4] Djoudi A, Bacha S, Iman-Eini H. Efficient real-time estimation for DFIG—performance and reliability enhancement of grid/micro-grid connected energy conversion systems. J Renew Sustain Energy. 2019;11(2).

[5] Mossa MA, Echeikh H, Quynh NV, et al. Performance dynamics improvement of a hybrid wind/fuel cell/battery system for standalone operation. IET Renew Power Gener. 2023;17(2):349–375. doi:10.1049/rpg2.12603

[6] Guo B, Bacha S, Alamir M, et al. Generalized integrator-extended state observer with applications to grid-connected converters in the presence of disturbances. IEEE Trans Control Syst Technol. 2020;29(2):744–755.

[7] Yaramasu V, Dekka A, Durán MJ, et al. PMSG-based wind energy conversion systems: survey on power converters and controls. IET Electr Power Appl. 2017;11(6):956–968. doi:10.1049/iet-epa.2016.0799

[8] LI L, Pei G, Liu J, et al. 2-DOF robust H-infty control for permanent magnet synchronous motor with disturbance observer. IEEE Trans Power Electron.

2021;36(3):3462–3472. doi:10.1109/TPEL.2020.3015874

[9] Yuan X, Chen J, Liu W, et al. A linear control approach to design digital speed control system for PMSMs. IEEE Trans Power Electron. 2022;37(7):8596–8610. doi:10.1109/TPEL.2022.3146174

[10] Jung J-W, Leu VQ, Do TD, et al. Adaptive PID speed control design for permanent magnet synchronous motor drives. IEEE Trans Power Electron. 2015;30(2):900–908. doi:10.1109/TPEL.2014.2311462

[11] Mayilsamy G, Natesan B, Joo YH, et al. Fast terminal synergetic control of PMVG-based wind energy conversion system for enhancing the power extraction efficiency. Energies. 2022;15(8):2774, doi:10.3390/en15082774

[12] Venkateswaran R, Yesudhas AA, Lee SR, et al. Integral sliding mode control for extracting stable output power and regulating DC-link voltage in PMVG-based wind turbine system. Int J Electr Power Energy Syst. 2023;144:108482. doi:10.1016/j.ijepes.2022.108482

[13] Kim S-K, Ahn CK. Active-damping speed tracking technique for permanent magnet synchronous motors with transient performance boosting mechanism. IEEE Trans Industr Inform. 2021;18(4):2171–2179.

[14] Alfehaid AA, Strangas EG, Khalil HK. Speed control of permanent magnet synchronous motor with uncertain parameters and unknown disturbance. IEEE Trans Control Syst Technol. 2021;29(6):2639–2646. doi:10.1109/TCST.2020.3026569

[15] Hao Z, Yang Y, Gong Y, et al. Linear/nonlinear active disturbance rejection switching control for permanent magnet synchronous motors. IEEE Trans Power Electron. 2021;36(8):9334–9347. doi:10.1109/TPEL.2021.3055143

[16] Kim S-K, Lee J-S, Lee K-B. Offset-free robust adaptive back-stepping speed control for uncertain permanent magnet synchronous motor. IEEE Trans Power Electron. 2015;31(10):7065–7076.

[17] Zhang X, He Y. Direct voltage-selection based model predictive direct speed control forPMSM drives without weighting factor. IEEE Trans Power Electron. 2019;34(8):7838–7851. doi:10.1109/TPEL.2018.2880906

[18] Liu M, Chan KW, Hu J, et al. Model predictive direct speed control with torque oscillation reduction for PMSM drives. IEEE Trans Industr Inform. 2019;15(9):4944–4956. doi:10.1109/TII.2019.2898004

[19] Preindl M, Bolognani S. Model predictive direct speed control with finite control set of PMSM drive systems. IEEE Trans Power Electron. 2013;28(2):1007–1015. doi:10.1109/TPEL.2012.2204277

[20] Kawai H, Zhang Z, Kennel R, et al. Direct speed control based on finite control set model predictive control with voltage smoother. IEEE Trans Ind Electron. 2023;70(3):2363–2372. doi:10.1109/TIE.2022.3174298

[21] Tu W, Luo G, Chen Z, et al. Predictive cascaded speed and current control for PMSM drives with multi-timescale optimization. IEEE Trans Power Electron. 2019;34(11):11046–11061. doi:10.1109/TPEL.2019.2897746

[22] Gao S, Wei Y, Zhang D, et al. Model-free hybrid parallel predictive speed control based on ultralocal model of PMSM for electric vehicles. IEEE Trans Ind Electron. 2022;69(10):9739–9748. doi:10.1109/TIE.2022.3159951

[23] Thounthong P, Sikkabut S, Poonnoy N, et al. Nonlinear differential flatness-based speed/torque control with state-observers of permanent magnet synchronous motor drives. IEEE Trans Ind Appl. 2018;54(3):2874–2884. doi:10.1109/TIA.2018.2800678

[24] Chaoui H, Khayamy M, Okoye O, et al. Simplified speed control of permanent magnet synchronous motors using genetic algorithms. IEEE Trans Power Electron. 2019;34(4):3563–3574. doi:10.1109/TPEL.2018.2851923

[25] Qu L, Qiao W, Qu L. An extended-state-observer-based sliding-mode speed control for permanent-magnet synchronous motors. IEEE J Emerg Sel Top Power Electron. 2020;9(2):1605–1613.

[26] Nguyen TH, Nguyen TT, Nguyen VQ, et al. An adaptive sliding-mode controller with a modified reduced-order proportional integral observer for speed regulation of a permanent magnet synchronous motor. IEEE Trans Ind Electron. 2022;69(7):7181–7191. doi:10.1109/TIE.2021.3102427

[27] Du H, Wen G, Cheng Y, et al. Design and implementation of bounded finite-time control algorithm for speed regulation of permanent magnet synchronous motor. IEEE Trans Ind Electron. 2020;68(3):2417–2426.